PCCP

Accepted Manuscript

ROYAL SOCIETY OF CHEMISTRY

www.rsc.org/pccp

Physical Chemistry Chemical Physics RSCPublishing

ARTICLE

A soft/hard magnetic nanostructure based on multisegmented CoNi nanowires

Cite this: DOI: 10.1039/xoxxoooooox

A. Pereira,[a] J. L. Palma,[a] M. Vázquez,[b] J. C. Denardin[a,c] and J. Escrig*[a,c]

Received ooth August 2014,
Accepted ooth January 2014

DOI: 10.1039/xoxxoooooox

www.rsc.org/nanoscale

In this paper we have introduced a new soft/hard nanostructure based on multisegmented CoNi nanowire arrays having diameters of around 110 nm and made of five segments with nominal compositions of Co, $Co_{66}Ni_{33}$, $Co_{50}Ni_{50}$, $Co_{33}Ni_{66}$ and Ni, each of which has a length of 800 nm, so that the total length of the multisegmented nanowire is 4 μm. These arrays have been synthesized by means of potentiostatic electrodeposition into the pores of hard-anodic alumina templates. Morphology, chemical composition and microstructure of the multisegmented CoNi nanowires were determined by high-resolution scanning electron microscopy, energy dispersive X-ray microanalysis, and powder X-ray diffraction method, respectively. The room temperature magnetic behavior of the multisegmented nanowire arrays is also studied and compared with CoNi nanowire arrays with homogeneous composition (non-segmented nanowires), synthesized in the same templates and having the same dimensions as the segmented ones. These nanostructures could be used to control the movement of magnetic domain walls. In this way, these nanostructures can be an alternative to store information or even perform logic functions.

A Introduction

The controlled movement of a number of domain walls along the nanowires using spin-polarized current pulses is the essential ingredient of racetrack memory[1], a technology that could store up to 100 times more data than existing random access memory (RAM). In racetrack memory, data are stored as a sequence of magnetic domains along a nanowire and individual bits are stored and retrieved by moving the sequence along the nanowire. When a spin-polarized current passes through a domain wall, the exchange interaction between conduction electrons and local magnetic moments gives rise to a spin-momentum transfer, which can move the domain wall along the nanowire[2]. Thus, racetrack memory uses electric currents to move magnetic domain walls up and down a nanowire without displacing any atoms at all. Of course, the spacing between consecutive domain walls (that is, the bit length) is controlled by pinning sites fabricated along the racetrack. As proposed by Parkin *et al.*[1], there are several means of creating such pinning sites; for example, by patterning notches along the edges of the racetrack or modulating the racetrack's size or material properties. Thus, the presence of pinning sites due to, for example, edges or rough surfaces may prevent the movement of domain walls. The release of static domain walls from pinning sites using current and/or external magnetic fields has been a widely studied topic[3-7]. The pinning or release of a domain wall has been shown to depend on the propagation mode of the domain wall[8,9].

Recently, Yan *et al.*[10] have presented numerical simulations on the motion of domain walls in cylindrical nanowires. They mentioned that the domain wall shown in these systems is very different from that observed in magnetic tapes, resulting in the absence of the drop in speed[11]. This introduces an advantage of the cylindrical systems in comparison with the magnetic tape. Thus, racetrack memories should consider cylindrical magnetic nanowires, which are synthesized by electrochemical deposition into porous alumina membranes. These membranes have attracted a huge scientific interest due to the outstanding features exhibited by these templates such as low cost, large self-ordering degree of the nanopores, high reproducibility and precise control over their morphological characteristics[12]. The main advantage of AAO templates lies in their customized geometrical features, such as nanopore diameter, length and center-to-center distance, which are easily controlled by tuning the anodization conditions[12,13].

Racetrack memories composed of cylindrical nanowires can create pinning sites by modulating the diameter of the nanowire[14-19], or considering multisegmented nanowires (different magnetic materials along the wire)[20-22]. Following these ideas, in this paper we have introduced a soft/hard magnetic nanostructure based on multisegmented CoNi nanowires, as shown in the left image of Fig. 2. The idea is to synthesize multisegmented nanowires where in each segment we have the possibility to finely control the magnetic parameters of the CoNi alloy by varying its stoichiometry. We have chosen CoNi segments because nanowires of this material have been found to exhibit outstanding properties since they can display either a soft or a hard magnetic behavior depending on the Co content in the alloy[23-27]. To date, there are only studies on multisegmented $Co_{56}Ni_{46}/Co_{85}Ni_{15}$ nanowire arrays with a diameter ranging between 180 and 200 nm and the length of each individual Co-Ni segment depending on its particular composition[28,29]. Despite these studies on multisegmented CoNi nanowire arrays, there is no report that synthesizes multisegmented nanowires where one end is nickel (it is well established that Ni nanowires present easy axes along the wire axis due to the predominant shape anisotropy contribution[30,31]), and where the segments go smoothly varying their stoichiometry until the last segment is cobalt (the case of Co is especially interesting due to its large magnetocrystalline anisotropy that favors in many cases a perpendicular-to-the-axis easy magnetization axis for the hcp equilibrium phase[32,33]). Furthermore, there is no report of the synthesis of multisegmented CoNi nanowires with diameter of 110 nm, and where all segments have the same length.

Geometrically, our multisegmented CoNi nanowires have a diameter of 110 nm and are composed of five segments of different material, each of which has a length of 800 nm, so that the total length of the multisegmented nanowire is 4 μm. The center-to-center distance between the multisegmented nanowires is 270 nm. Thus, in this paper we present the synthesis of multisegmented nanowires composed by segments with nominal compositions of Co, $Co_{66}Ni_{33}$, $Co_{50}Ni_{50}$, $Co_{33}Ni_{66}$ and Ni based on ordered aluminum oxide membranes, and the morphological, crystallographic and magnetic characterization are shown.

B Experimental details

Multisegmented CoNi nanowire arrays were synthesized by electrochemical deposition into anodic aluminum oxide (AAO) membranes used as templates. The synthesis was performed in 0.32-mm-thickness electropolished Al foils (99.999% pure from GoodFellow), which were pre-anodized in a 0.3 M oxalic acid under a voltage of 40 V for 10 min. Afterwards, the anodization voltage was increased at 0.08 V/s to reach potentiostatic conditions in the hard anodization (HA) process, which was carried out at 140 V for 50 min[26,34]. All these HA processes were performed at 0 ºC. The obtained AAO is characterized by the presence of an array of self-ordered nanopores with a diameter *d* of about 110 nm, arranged in a dense hexagonal lattice with a periodicity of ~270 nm (see Fig. 1(a)).

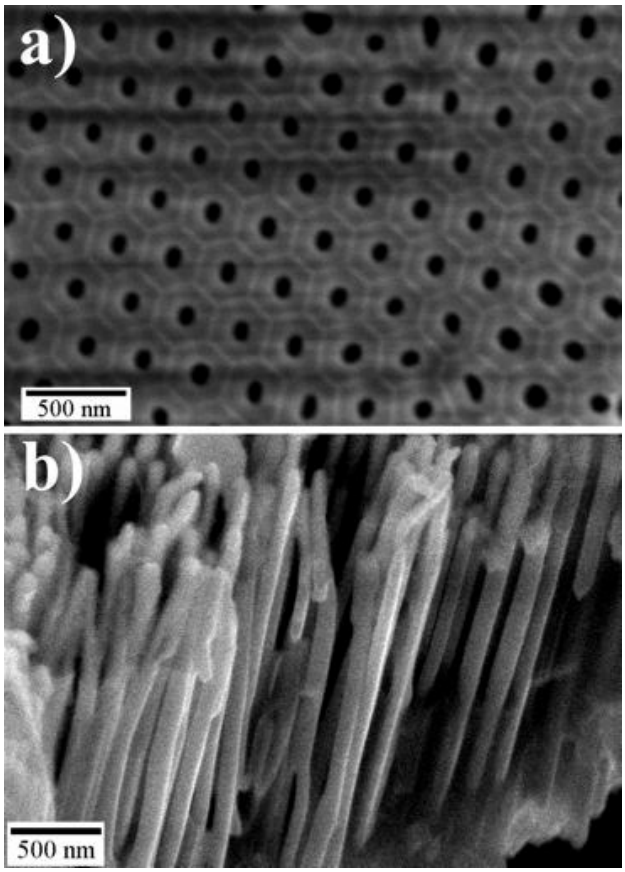

Figure 1 (a) SEM image of the porous alumina membrane used as a template for the electrochemical synthesis of the multisegmented CoNi nanowire arrays displaying the hexagonally ordered pore distribution with 110 nm in size and pore inter-spacing of around 270 nm. (b) SEM cross-sectional view of multisegmented CoNi nanowires released from the template

In order to obtain a conductive layer for the electrodeposition, the aluminum and barrier layers were selectively removed from the bottom of the membranes by chemical etching and a 150-nm Ag layer was sputtered to form the electrode. The AAO is then used as a template for the growth of multisegmented CoNi nanowire arrays, where nickel and cobalt salts were used in different proportions (see Table 1) to produce solutions that were electrodeposited inside the nanopores of alumina. The pH of the solutions was 3.5 and the electrodeposition temperature was 35 ºC. This process was performed in the potentiostatic mode at 1.3 V for 1 min for the growth of each segment. Among the electrodeposition of each segment, we rinsed the deposit cell with distilled water and ethanol, and then we dried it before starting a new electrodeposition.

Electrolyte composition (g/l)				
Composition		Salts		
Nominal	Measured	$CoSO_4 \cdot 7H_2O$	$NiSO_4 \cdot 7H_2O$	H_3BO_4
Co	$Co_{96.62}Ni_{3.38}$	300	0	45
$Co_{66}Ni_{33}$	$Co_{82.44}Ni_{17.56}$	50	200	45
$Co_{50}Ni_{50}$	$Co_{50.73}Ni_{49.27}$	30	300	45
$Co_{33}Ni_{66}$	$Co_{26.64}Ni_{76.36}$	10	300	45
Ni	$Co_{2.72}Ni_{97.28}$	0	300	45

Table 1 Solutions used for electrodeposition of multisegmented CoNi nanowire arrays. "Measured" column corresponds to those ratios obtained by EDX.

The morphology, chemical composition and microstructure of the samples were studied by high-resolution scanning electron microscopy (HRSEM, FEI Nova Nano 230), energy dispersive X-ray microanalysis (EDX) and powder X-ray diffraction (XRD) method (Philips X-Pert diffractometer), respectively. All magnetic measurements were performed in an EZ-7 commercial vibrating-sample magnetometer. Measurements were done at room temperature as a function of the angle between the applied field and the multisegmented CoNi nanowire under a maximum applied field of 10 kOe.

C Results and discussion

Figure 1(a) shows a scanning electron microscope (SEM) image of a typical AAO layer used for the electrochemical synthesis of the multisegmented CoNi nanowire arrays, indicating the uniformity of the pore size (d = 110 nm) and pore interspacing (D = 270 nm) of highly ordered surface pore distribution with hexagonal symmetry achieved during the hard anodization process. Pore filling of these templates was performed by electrochemical deposition of CoNi alloys, with controlled composition under potentiostatic conditions. Figure 1(b) shows a SEM image of a cross-sectional view of multisegmented CoNi nanowires released from the template, where the sequence of segments with alternating CoNi alloy composition is visible due to their differences in composition.

The left image of Fig. 2 shows the schematic illustration of our multisegmented CoNi nanowires. They are composed of five segments of different material (nominally we expected Co, $Co_{66}Ni_{33}$, $Co_{50}Ni_{50}$, $Co_{33}Ni_{66}$ and Ni), each of which has a length of 800 nm, so that the total length of the multisegmented nanowire is 4 μm. To verify the distribution of the two elements within the multisegmented CoNi nanowires, EDX mapping of the nickel and cobalt elements were investigated. The center image of Fig. 2 shows the areas of a SEM image for multisegmented CoNi nanowires which were used for the chemical analysis (marked by the yellow dashed rectangle). From the right image of Fig. 2 we can see that the Ni and Co elements are distributed gradually, thereby obtaining a smooth transition from one end of the nanowire (nickel) to the other (cobalt). The compositions shown in the right image of Fig. 2 have been obtained from the EDX spectrum analyzed in Fig. 3. Importantly, the experimentally measured compositions are not exactly those that we wanted to synthesize, which is probably ascribed to relaxation effects that occur during the deposition processes, as well as the selected window for EDX spectrum consider more than one segment of the multisegmented nanowires. Finally, from the right image of Fig. 2 is clearly observed the soft/hard structure of our multisegmented CoNi nanowires.

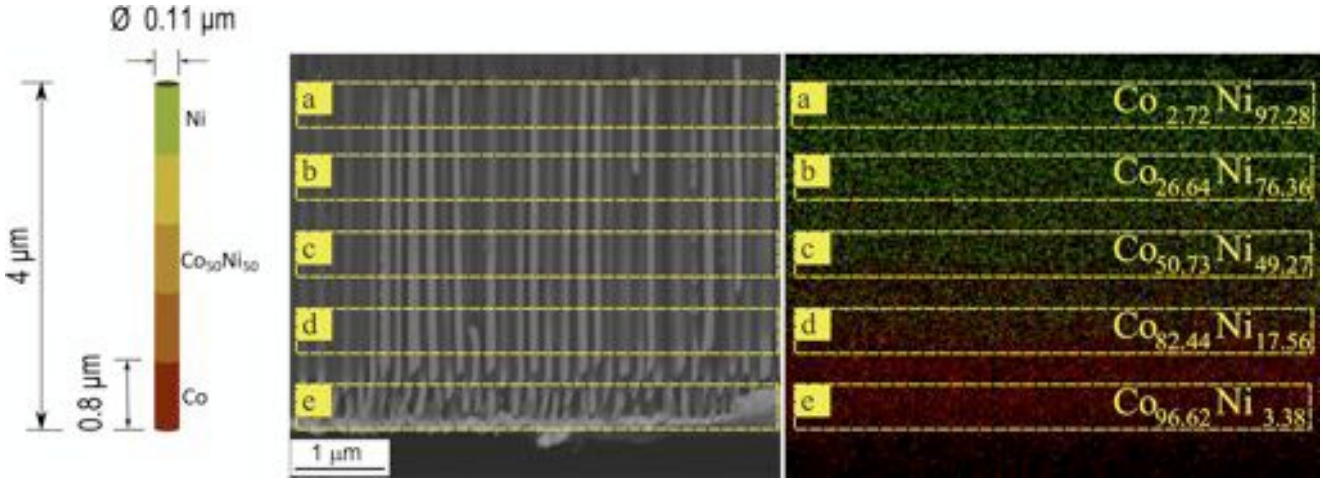

Figure 2 (Left) Schematic illustration of a multisegmented CoNi nanowire where the composition varies smoothly in the system from a soft magnetic material (nickel) to a hard magnetic material (cobalt). (Center) SEM cross-sectional view of multisegmented CoNi nanowires grown into the nanoporous template, of which the yellow dashed rectangles shows the scanning area of the elemental mapping. (Right) EDX elemental mappings of Ni Kα and Ni Kβ (green points), and Co Kα and Co Kβ (red points).

Physical Chemistry Chemical Physics RSCPublishing

ARTICLE

The chemical composition of the multisegmented CoNi nanowire arrays was determined by analyzing the EDX spectra obtained from a cross-sectional SEM image (see the center image of Fig. 2). Figure 3 shows the EDX spectra recorded from the five different segments identified in the right image of Fig. 2.

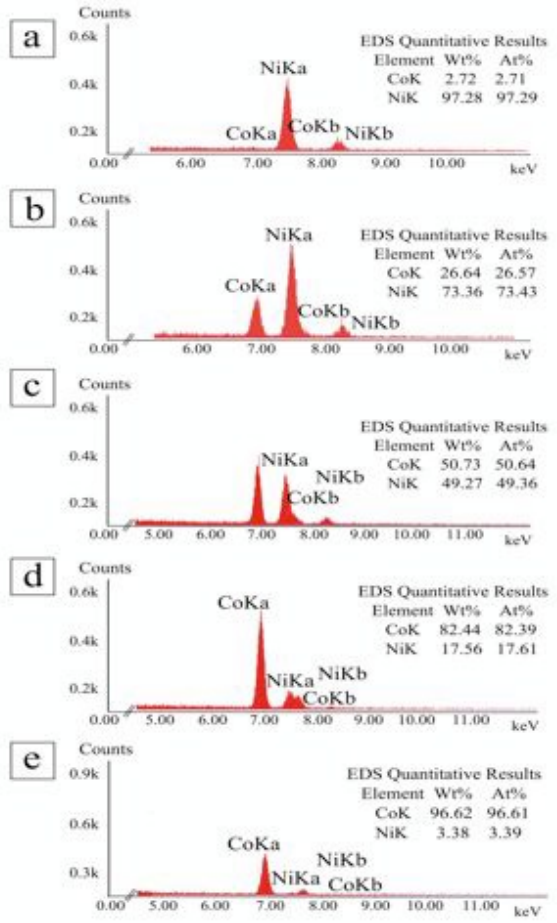

Figure 3 EDX spectra acquired from five different segments identified in the center image of Fig. 2.

EDX spectra for all windows (a-e) show peaks corresponding to the elements nickel and cobalt, consistent with the expected compositions of the multisegmented CoNi nanowires. From these EDX spectra is clear that for the window (a) we have a well-defined Ni Kα peak at 7.478 keV. Quantitative analysis indicates a 3:97 atomic ratio of Co:Ni, referring to a Co_3Ni_{97} composition. In the window (b) we observed the appearance of a peak corresponding to Co Kα at 6.980 keV, but clearly smaller than the Ni Kα peak. Quantitative analysis indicates a 27:73 atomic ratio of Co:Ni, referring to a $Co_{27}Ni_{73}$ composition. In the window (c) we observed that both the Ni Kα and Co Kα peaks are approximately equal. In fact, a quantitative analysis indicates a 51:49 atomic ratio of Co:Ni, referring to a $Co_{51}Ni_{49}$ composition. In the window (d) we observed that clearly the Co Kα peak is much higher than the Ni Kα peak. This can be verified with the quantitative analysis, which indicates a 82:18 atomic ratio of Co:Ni, referring to a $Co_{82}Ni_{18}$ composition. Finally, in the window (e) we observed that clearly highlights the Co Kα peak. Quantitative analysis indicates a 97:3 atomic ratio of Co:Ni, referring to a $Co_{97}Ni_3$ composition. Thus, we have synthesized an array of multisegmented nanowires where one end is about 97% nickel (soft magnetic material), while the other end has the same percentage of cobalt (hard magnetic material). The intensities of the Ni Kα and Co Kα peaks vary along the multisegmented nanowire as expected.

In order to perform a detailed structural characterization of each of the segments of the multisegmented nanowires, we have synthesized new samples of nanowires, one for each of the compositions of the segments defined in Table 1. These arrays have been synthesized considering the same dimensions as the multisegmented nanowire arrays (110 nm pore size and 270 nm pore interspacing of highly ordered surface pore distribution). Figure 4 displays the X-ray diffraction (XRD) patterns corresponding to the Co, $Co_{66}Ni_{33}$, $Co_{50}Ni_{50}$, $Co_{33}Ni_{66}$, and Ni nanowire arrays, from top to bottom. For the Co nanowire sample, only the hcp-phase (100), (002) and (101) peaks are detected [Fig. 4(a)]. With the addition of Ni, the size of the hcp (100) and (101) Co peak decrease significantly. Instead, the (111) Ni peak is observed [Fig. 4(b)]. By further increasing the ratio of nickel, cobalt peaks completely disappear, and (200) and (220) Ni peaks appear [Figs. 4(c)-4(d)]. This behavior indicates that the crystal structure of the segments of a multisegmented nanowire evolved from an hcp phase (cobalt-rich segment) to a fcc phase (nickel-rich segment).

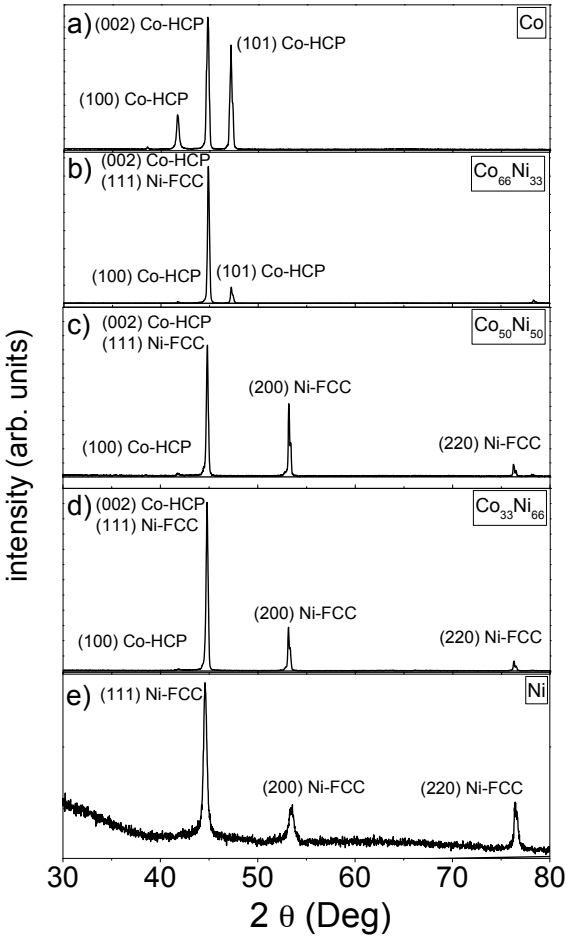

Figure 4 XRD θ-2θ diffraction patterns of (a) Co, (b) $Co_{66}Ni_{33}$, (c) $Co_{50}Ni_{50}$, (d) $Co_{33}Ni_{66}$, and (e) Ni nanowires.

An interesting aspect to be explored is the angular dependence of the magnetization. Magnetic hysteresis loops were measured at different angles (θ) between the external magnetic field (H) and the multisegmented nanowire long axis. Figure 5 shows the magnetic hysteresis loops measured for the multisegmented CoNi nanowire array, with d = 110 nm. From this, we observed that both the coercivity and the remanence decreased as we increased the angle at which the external field is applied. It is also interesting to note the slight widening that occurs in the hysteresis curve when the magnetization approaches zero (see insert image in Fig. 5). This effect is present for angles smaller than 45º, and its origin may be due to various compositions comprising the multisegmented nanowire, which obviously have different coercivities[27]. In addition, it is interesting to note the non-monotonic behavior exhibiting hysteresis curves when they approach the saturation magnetization. Finally, the remanence takes generally small values at all angles, so the contribution from magnetostatic interactions may be relevant. However, there is an effective axial magnetization easy axis, parallel to the wires.

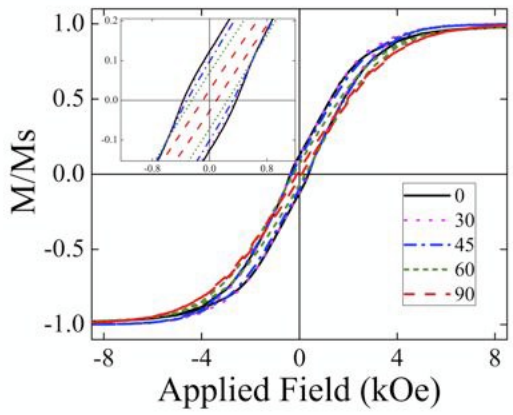

Figure 5 Room temperature normalized magnetization for the multisegmented CoNi nanowire array schematized in the left image of Figure 2, recorded using a VSM as a function of the angle θ in which the external magnetic field is applied. The inset image shows a zoom of the hysteresis curves to see in detail the behaviour of remanence and coercivity of the array.

In Figure 6 we summarized the coercivity H_c and relative remanence M_r/M_s of the multisegmented CoNi nanowires (see black squares) measured for different θ values. We observed a significant dependence of the magnetic properties on θ. In particular, the coercive field can be tuned between 100 to 380 Oe approximately by properly adjusting θ. Furthermore, the dependence of the coercivity is nonlinear (the coercivity remained approximately stable between 0 and 30º, and then abruptly decreased for further increases in the angle).

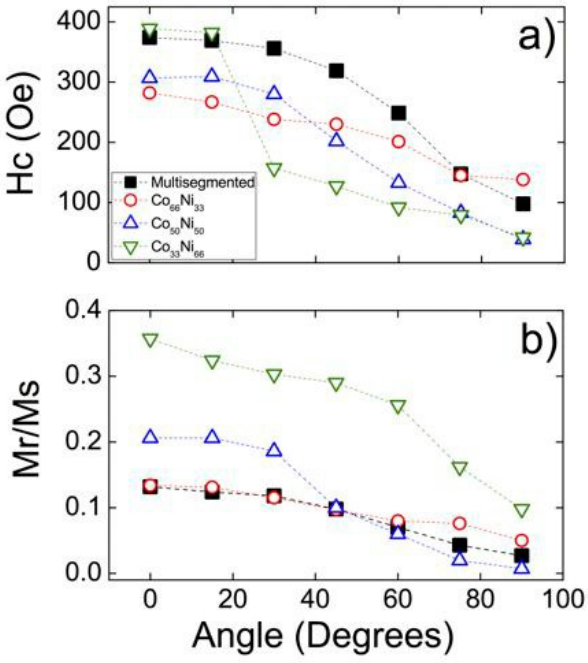

Figure 6 (a) Coercivity and (b) relative remanence for multisegmented CoNi nanowire arrays (black squares), homogeneous $Co_{66}Ni_{33}$ nanowire arrays (red circles), homogeneous $Co_{50}Ni_{50}$ nanowire arrays (blue triangles) and homogeneous $Co_{33}Ni_{66}$ nanowire arrays (green inverted triangles) as a function of θ.

It is interesting to note that although there are segments of different compositions, the minimum energy configuration of them appears when the multisegmented nanowire reverses its magnetization by nucleation and propagation of a vortex domain wall[35]. This due to the nanowire exhibits a diameter of 110 nm. Moreover, when the applied field is reduced to zero, at remanence, the magnetization is measured at the θ angle with respect to the easy axis. Thus, we can observe that the remanence follows the function $M_r(\theta) = M_r\cos^2(\theta)$, with $M_r = M_r(\theta = 0)$ the remanence measured at $\theta = 0º$. Besides, we observe a quasi-unhysteretic behavior for $\theta = 90º$. This behavior allows us to conclude that shape anisotropy of multisegmented CoNi nanowires may induce a hard axis of magnetization when $\theta = 90º$.

Finally, it is important to make a comparison between homogeneous CoNi nanowire arrays and multisegmented CoNi nanowire arrays. To do this, we have measured the magnetic properties of homogeneous CoNi nanowires, synthesized in the same templates and having the same dimensions as the segmented ones. Figure 6 also shows the coercivity and remanence for these homogeneous CoNi nanowire arrays. From these results we have obtained that the multisegmented CoNi nanowire array exhibits a coercivity very similar to that obtained by the $Co_{33}Ni_{66}$ nanowire array when $\theta < 20º$. However, for the range between $20° < \theta < 70º$ we obtained an unexpected behaviour because the coercivity of the multisegmented CoNi nanowire array is higher than those measures for homogeneous CoNi nanowire arrays. Thus, for potential applications requiring high coercivity is better to use a multisegmented nanowire array than a homogeneous nanowire array, within the range of $20° < \theta < 70º$. Finally, we obtained that the multisegmented CoNi nanowire array exhibits a coercivity very similar to that obtained by the $Co_{66}Ni_{33}$ nanowire array when $\theta > 70º$. From these results we can conclude that for small angles the system behaves as a nickel-rich system, while for large angles, the system behaves as a cobalt-rich system. Finally, we have obtained that the multisegmented CoNi nanowire array exhibits a remanence very similar to that obtained by the $Co_{66}Ni_{33}$ nanowire array for the entire range of angles investigated.

Conclusions

In conclusion, multisegmented CoNi nanowire arrays, with around 110 nm in diameter and made of five segments of different material ($Co_{97}Ni_3/Co_{82}Ni_{18}/Co_{51}Ni_{49}/Co_{27}Ni_{73}/Co_3Ni_{97}$), each of which has a length of 800 nm, so that the total length of the multisegmented nanowire is 4 μm, have been synthesized by template-assisted electrochemical deposition in hard-anodic alumina templates by varying the solutions prepared of different proportions of nickel and cobalt salts. The change in the composition along the multisegmented nanowires enables to tune the magnetic properties of each segment as the Co content is increased. In particular, we have investigated the angular dependence of the magnetic properties of multisegmented CoNi nanowire arrays. We observed a significant dependence of the magnetic properties on θ. In particular, we observed that both the coercivity and the remanence decrease as we increase the angle at which the external field is applied. Besides, we observed a slight widening that occurs in the hysteresis curve when the magnetization approaches zero (see insert image in Fig. 5). Additionally, we obtained that the coercive field can be tuned between 100 to 380 Oe approximately by properly adjusting θ. Besides, we observed a quasi-unhysteretic behavior for $\theta = 90º$. Furthermore, we compared the magnetic properties between homogeneous CoNi nanowire arrays and multisegmented CoNi nanowire arrays and we realized that for small angles the multisegmented system behaves as a nickel-rich homogeneous system, while for large angles, the multisegmented system behaves as a cobalt-rich homogeneous system. Finally, the ability to tune the compositions along a multisegmented CoNi nanowire should enable one to highlight novel aspects that may be useful for potential applications.

Acknowledgements

In Chile, we acknowledge support from Fondecyt under projects 3140073, 3130393, 1110784 and 1140195, Grant ICM P10-061-F by Fondo de Innovación para la Competitividad-Minecon and the Financiamiento Basal para Centros Científicos y Tecnológicos de Excelencia, under project FB0807. In Spain, we thank the Spanish Ministry of Economía y Competitividad, MEC, under project i-LINK0783.

Notes and references

[a] Avenida Ecuador 3493, Departamento de Física, Universidad de Santiago de Chile, 9170124 Santiago, Chile.
[b] Institute of Materials Science of Madrid, CSIC, 28049 Madrid, Spain.
[c] Avenida Ecuador 3493, Center for the Development of Nanoscience and Nanotechnology, 9170124 Santiago, Chile.

1 S. S. P. Parkin, M. Hayashi and L. Thomas, Science, 2008, 320, 190-194.
2 L. Thomas, R. Moriya, C. Rettner and S. S. P. Parkin, *Science*, 2010, **330**, 1810-1813.

3 L. Thomas, M. Hayashi, X. Jian, R. Moriya, C. Rettner and S. S. P. Parkin, *Nature*, 2006, **443**, 197-200.
4 L. Thomas, M. Hayashi, X. Jiang, R. Moriya, C. Rettner and S. Parkin, *Science*, 2007, **315**, 1553-1556.
5 M. Hayashi, L. Thomas, C. Rettner, R. Moriya, X. Jiang and S. S. P. Parkin, *Phys. Rev. Lett.*, 2006, **97**, 207205.
6 D. Bedau, M. Klaeui, S. Krzyk and U. Ruediger, *Phys. Rev. Lett.,* 2007, **99**, 146601.
7 K. -J. Kim, J. Ryu, G. –H. Gim, J. –C. Lee, K. –H. Shin, H. –W. Lee and S. –B. Choe, *Phys. Rev. Lett.*, 2011, **107**, 217205.
8 H. Tanigawa, T. Koyama, M. Bartkowiak, S. Kasai, K. Kobayashi, T. Ono and Y. Nakatani, *Phys. Rev. Lett.*, 2008, **101**, 207203.
9 S. –M. Ahn, K. –W. Moon, D. –H. Kim and S. –B. Choe, *Appl. Phys. Lett.*, 2009, **95**, 152506.
10 M. Yan, A. Kakay, S. Gliga and R. Hertel, *Phys. Rev. Lett.*, 2010, **104**, 057201.
11 G. Beach, C. Nistor, C. Knutson, M. Tsoi and J. Erskine, *Nat. Mater.*, 2005, **4**, 741-744.
12 H. Masuda and K. Fukuda, *Science*, 1995, **268**, 1466-1468.
13 K. Nielsch, J. Choi, K. Schwirn, R. B. Wehrspohn and U. Gosele, *Nano Lett*., 2002, **2**, 677-680.
14 S. Allende, D. Altbir and K. Nielsch, *Phys. Rev. B*, 2009, **80**, 174402.
15 K. Pitzschel, J. Bachmann, S. Martens, J. M. Montero-Moreno, J. Kimling, G. Meier, J. Escrig, K. Nielsch and D. Goerlitz, *J. Appl. Phys.*, 2011, **109**, 033907.
16 A. Rotaru, J. –H. Lim, D. Lenormand, A. Diaconu, J. B. Wiley, P. Postolache, A. Stancu and L. Spinu, *Phys. Rev. B*, 2011, **84**, 134431.
17 M. S. Salem, P. Sergelius, R. Zierold, J. M. M. Moreno, D. Goerlitz and K. Nielsch, *J. Mater. Chem*., 2012, **22**, 8549-8557.
18 M. S. Salem, P. Sergelius, R. M. Corona, J. Escrig, D. Goerlitz and K. Nielsch, *Nanoscale*, 2013, **5**, 3941-3947.
19 I. Minguez-Bacho, S. Rodriguez-López, M. Vázquez, M. Hernández-Vélez and K. Nielsch, *Nanotechnology*, 2014, **25**, 145301.
20 W. Lee, R. Scholz, K. Nielsch and U. Goesele, *Angew. Chem. Int. Ed*., 2005, **44**, 6050-6054.
21 M. A. Bangar, C. M. Hangarter, B. Yoo, Y. Rheem, W. Chen, A. Mulchandani and N. V. Myung, *Electroanalysis*, 2009, **21**, 61-67.
22 B. Leighton, O. J. Suarez, P. Landeros and J. Escrig, *Nanotechnology*, 2009, **20**, 385703.
23 S. Talapatra, X. Tang, M. Padi, T. Kim, R. Vajtai, G. V. S. Sastry, M. Shma, S. C. Deevi and P. M. Ajayan, *J. Mater. Sci*., 2009, **44**, 2271-2275.
24 M. Vázquez and L. G. Vivas, *Phys. Status Solidi B*, 2011, **248**, 2368-2381.
25 L. G. Vivas, M. Vázquez, J. Escrig, S. Allende, D. Altbir, D. C. Leitao and J. P. Araujo, *Phys. Rev. B*, 2012, **85**, 035439.
26 V. Vega, T. Bohnert, S. Martens, M. Waleczek, J. M. Montero-Moreno, D. Gorlitz, V. M. Prida and K. Nielsch, *Nanotechnology*, 2012, **23**, 465709.
27 A. Pereira, C. Gallardo, A. P. Espejo, J. Briones, L. G. Vivas, J. C. Denardin and J. Escrig, *J. Nanopart. Res*., 2013, **15**, 2041.
28 V. M. Prida, J. García, L. Iglesias, V. Vega, D. Goerlitz, K. Nielsch, E. D. Barriga-Castro, R. Mendoza-Reséndez, A. Ponce and C. Luna, *Nanoscale Research Letters*, 2013, **8**, 263.
29 J. García, V. Vega, L. Iglesias, V. M. Prida, B. Hernando, E. D. Barriga-Castro, R. Mendoza-Reséndez, C. Luna, D. Goerlitz and K. Nielsch, *Phys. Status Solidi A*, 2014, **211**, 1041-1047.
30 K. Ounadjela, R. Ferre, L. Louail, J. M. George, J. L. Maurice, L. Piraux and S. Dubois, *J. Appl. Phys*., 1997, **81**, 5455.
31 X. Xu and G. Zangari, *J. Appl. Phys*., 2005, **97**, 10A306.
32 J. Cho, J. Hyun, J. H. Wu, S. P. Min, J. Y. Ko, Q. X. Soh and Y. K. Kim, *J. Magn. Magn. Mater*., 2006, **303**, e281-e285.
33 Y. P. Ivanov, L. G. Vivas, A. Asenjo, A. Chuvillin, O. Chubykalo-Fesenko and M. Vázquez, *EPL*, 2013, **102**, 17009.
34 W. Lee, R. Ji, U. Goesele and K. Nielsch, *Nature Mater*., 2006, **5**, 741- 747.
35 P. Landeros, S. Allende, J. Escrig, E. Salcedo, D. Altbir and E. E. Vogel, *Appl. Phys. Lett.,* 2007, **90**, 102501.